archaeometry

*Archaeometry* **54**, 3 (2012) 528–548 doi: 10.1111/j.1475-4754.2011.00631.x

# ARCHAEOMETALLURGICAL CHARACTERIZATION OF HELLENISTIC METAL OBJECTS: THE CONTRIBUTION OF THE BRONZE OBJECTS FROM RISHON LE-ZION (ISRAEL)*

D. ASHKENAZI† and N. IDDAN

*Faculty of Engineering, Tel Aviv University, Ramat Aviv, 69978, Israel*

and O. TAL

*Department of Archaeology and Ancient Near Eastern Cultures, Tel Aviv University, Ramat Aviv, 69978, Israel*

*An archaeometallurgical analysis is presented of 14 bronze artefacts retrieved from an Early Hellenistic–period farmstead in controlled archaeological excavations at Rishon Le-Zion, Israel, and dated to the first quarter of the third century BCE according to coins and pottery vessels. The bronze assemblage includes a needle, pins, spatulas and fibulas. The aims of the research are to determine the composition, microstructure and manufacturing process of these artefacts, and to discover their place of production. This will provide a better understanding of Hellenistic technological abilities and material culture. The examination included optical microscopy, microhardness, SEM including EDS, and XRD. The results show that the collection consists of Cu–Sn binary alloys, with evidence for a controlled alloying process and the absence of recycling. Furthermore, the microstructure of the objects indicates that all artefacts were produced by a cold-working process. Moreover, the manufacturing process of the rectangular cross-section fibulas included sophisticated joining techniques of copper and iron.*

*KEYWORDS:* ARCHAEOMETALLURGY, METALLOGRAPHY, BRONZE, HELLENISTIC, ISRAEL

## INTRODUCTION

The finds discussed in this paper originated from a site called Holot Rishon Le-Zion (South) (Israeli Map Ref. 1275 1525) that is geologically located upon the Gaza Formation, which is of the Quaternary Age. Prior to the excavations, the site was covered by a thick layer of migrating sand dunes, stabilized in part by plants, and containing terrestrial snails, plant remains, a few animal bones and pottery, deposited in the last three to four thousand years and, therefore, it was never mentioned by the surveyors of ancient Palestine. This layer of sand dunes makes up part of the geological unit of the Hadera Dune Bed (Rishon Le-Zion Deposit), dominated by dunal morphology with typical cross-bedding. This unit apparently overlies most of the archaeological sites along the southern Sharon plain and northern Philistia, and is usually characterized by shrubs. Erosion sometimes removes this upper unit, thereby exposing the Tel Aviv Kurkar (fossilized dune sandstone) Bed or the Ta'arukha Hamra Bed underneath, and revealing archaeological sites (Fig. 1).

The site was discovered by inspectors of the Israel Antiquities Authority after having been exposed by mechanical tools while the area was being prepared for residential building

*Received 24 October 2010; accepted 14 July 2011
†Corresponding author: email dana@eng.tau.ac.il

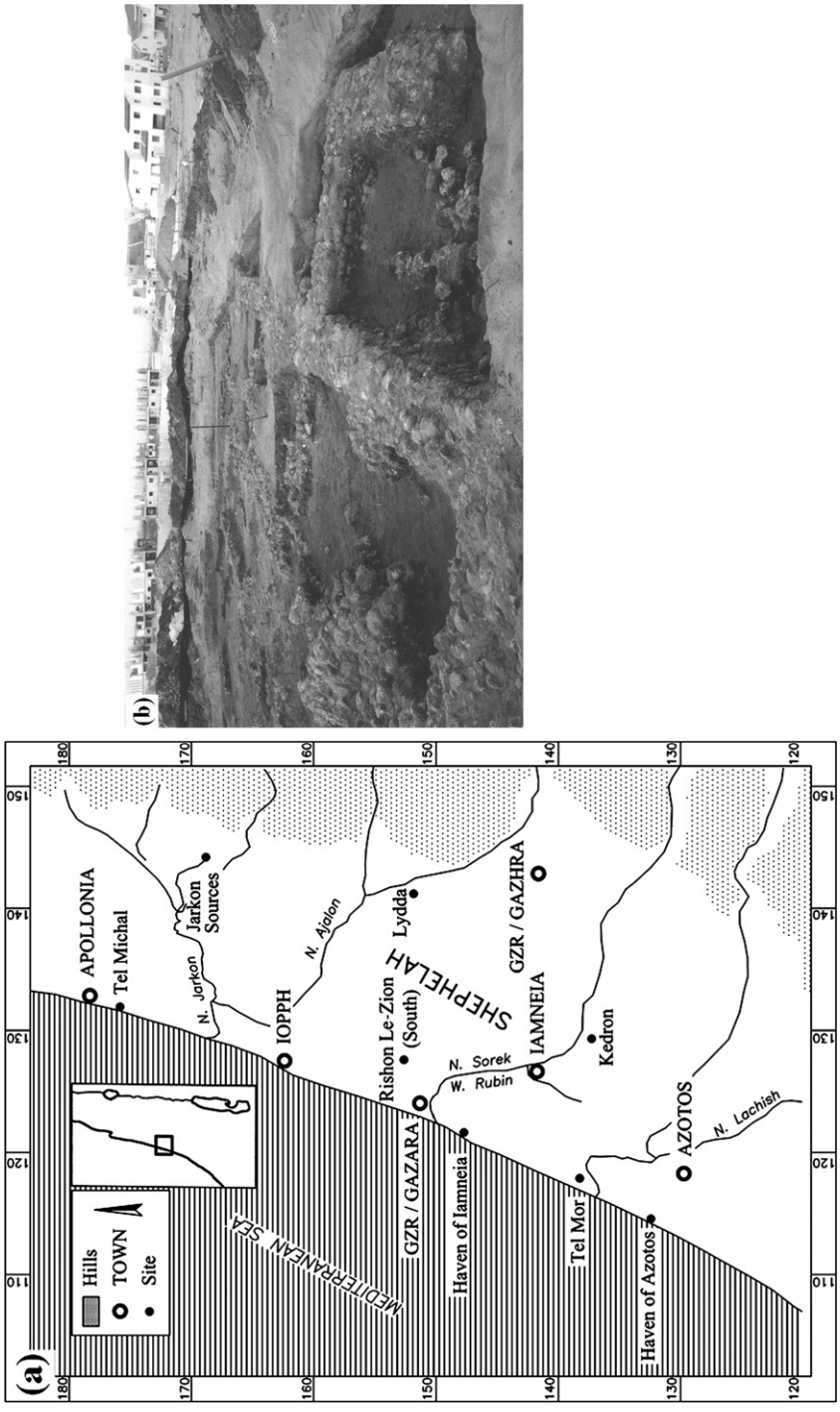


Figure 1 *The Rishon Le-Zion archaeological excavations: (a) a location map of the site; (b) a general view, looking east.*

operations. After a trial excavation had been conducted on behalf of the Israel Antiquities Authority, a rescue excavation was carried out by Tel Aviv University, revealing three strata of occupation dating to the fifth to third centuries BCE (Tal 2005). The earlier stratum (Stratum III) was characterized by round or square pits of varying sizes, hewn in the local rock, which usually forms part of the Tel Aviv Kurkar Bed. The nature of Stratum III was of storage, as the pits were most likely connected with the storing of grains. The middle stratum (Stratum II) was characterized by walls built of sun-dried mud bricks, red loam (*ḥamra*) soil mixed with grits, and organic matter without stone foundations that had simply been placed after Stratum III was levelled, at some points down to bedrock. The remains of Stratum II seem to belong to a farmstead, the nature of which is still uncertain. The limited extent of excavations and finds in both Strata III and II enables them to be dated to either the fifth or the fourth century BCE.

The architectural remains of the upper, late stratum (Stratum I), from which the bronze objects discussed in this paper were retrieved, formed part of a farmhouse (approx. 21 × 23 m) built with field-stone walls (Fig. 2). The farmstead contained a central courtyard in the south and rooms around three sides at least, with two rows of rooms on the northern side. In the centre of the northern wall was an entrance (width approx. 0.75 m), which led to an antechamber. A number

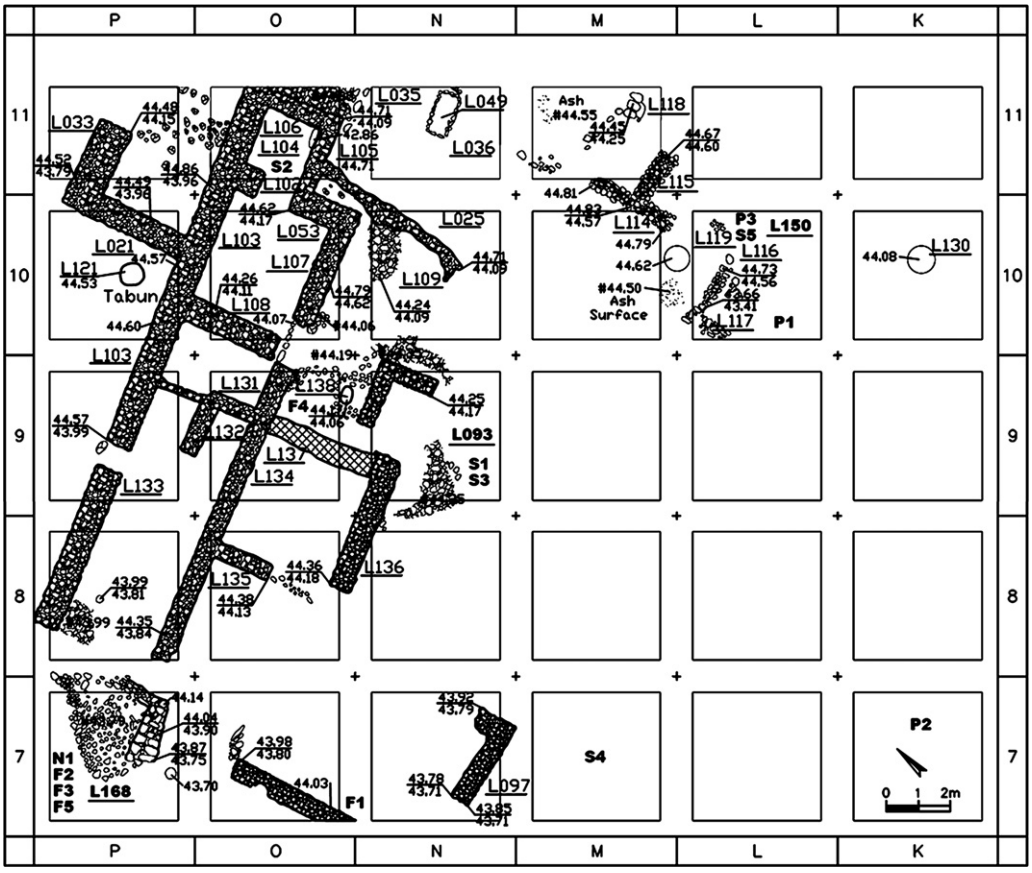


Figure 2 *A plan of the farmstead at Rishon Le-Zion, with an indication of the spatial location of the analysed metal artefacts.*

of rooms had a beaten-earth floor, and in others the floor was composed of small field stones. *Ṭābūns* (ovens), various installations and grinding tools were found mainly in the eastern rooms, and hearths were found in the courtyard. *Ṭābūns* and other installations were also found outside the building. Some walls were built on top of the brick walls of Stratum II. Two phases were uncovered in the stone structure (Ia and Ib), in the form of repairs and additions to the walls in some of the rooms. Most of the finds uncovered in the building consisted of numerous pottery vessels (mainly tableware), metal (bronze and iron) artefacts including work and hunting tools as well as weaponry, items of clothing and cosmetics (the pins, spatulas and fibulas, below), jewellery and metal-working tools (the needle, below). A stamped handle of a Rhodian amphora (that reads 'Aristo[ . . . '), dated to the first quarter of the third century BCE, along with two posthumous coins of Alexander the Great (post–323 BCE) and 20 coins of Ptolemy I (the latest coins may be dated to 283 BCE), suggest an occupation of a few decades in the last quarter of the fourth century and/or the first quarter of the third century BCE. This date agrees with all the finds recovered from the site. It seems that the site was abandoned in the 280s/270s BCE for yet-to-be-discovered reasons. The settlement archaeology and geographical history of the primary site of the region, Tel Ya'oz (GZR/GAZHARA of Fig. 1), in Persian and Hellenistic times, has been discussed at some length elsewhere (cf., Fischer *et al*. 2008; Tal 2009).

## ARCHAEOMETALLURGICAL BACKGROUND

Archaeometallurgical methods will assist us in learning about the manufacturing process of the Rishon Le-Zion artefacts, as well as in answering research questions such as whether the artefacts were produced locally. These methods may also give us an opportunity to learn more about the Hellenistic material culture and copper-trade trends during the Hellenistic period. Copper (Cu) alloys have been used in a variety of applications since antiquity. Small additions of tin (Sn) to Cu considerably reduce the melting point of the alloy and improve the mechanical properties. Bronzes in antiquity usually contain up to 15 wt% Sn. A higher tin content improves the bronze's castability, but also increases the embrittlement due to the $\alpha + \delta$ eutectoid phase formation (Meeks 1986; Srinivasan 1998).

A combination of typological groups and chemical compositions may assist in determining the origin of archaeological artefacts as well as the provenance of their raw materials (Craddock and Giumlia-Mair 1988). Archaeological studies of Cu artefacts of the second to first millennia BCE in Western Europe show that they were manufactured based on the use of bronze technology. The composition of the alloy depends on the raw materials as well as on the smelting process (including trace elements from the fluxes, ore and fuels) and the alloying technologies at the metalworking centres (Craddock and Giumlia-Mair 1988). Late Bronze Age metallic objects from Atlantic Europe were made of leaded bronzes and contained more than 2 wt% Pb, whereas European regions around the Mediterranean Sea, such as Greece and Italy, were using mostly a binary Cu–Sn alloy (Vale'rio *et al*. 2010). Leaded bronze bangles (1000 to 450 BCE) excavated from Tell en-Naṣbeh, northern Judah, revealed an economic relationship with Edom (Friedman *et al*. 2008).

The composition of a Hellenistic bronze naval ram found south of Haifa (Athlit Bay), Israel, revealed the presence of 90.4% Cu and 9.6% Sn, without any Pb (Oron 2006). There are no major differences between tools, jewellery and ornaments, although objects with a high concentration of tin (~13–15 wt% Sn) are non-functional prestige objects (Vale'rio *et al*. 2010). During the second to first millennia BCE, the Mediterranean regions imported raw materials, including tin, from neighbouring areas (Giumlia-Mair 2005; Vale'rio *et al*. 2010). The high Sn concentration of

bronze artefacts gives them a more yellowish-brown hue, which may have been considered more suitable for prestige objects (Giumlia-Mair 2005; Vale'rio *et al*. 2010). The manufacture of an artefact from low-tin bronze means combining ductility and hardenability, as well as good strength and fracture toughness (Ponting and Segal 1998; Ponting 2002a,b). Very low-tin bronze (less than 2 wt% Sn) indicates recycling (Rovira and Montero 2003; Vale'rio *et al*. 2010). Ponting studied Roman military copper alloy artefacts of the first century CE, including two types of fibulas from Masada and Gamla, Israel (Ponting and Segal 1998; Ponting 2002a,b). The elbow fibulas from both Masada and Gamla were all made of tin bronze (8–10 wt% Sn). Tin, lead and zinc were the major alloying elements found in the Cu-alloy artefacts from Masada. Those elements are typical of Roman military bronze objects excavated at European sites (Ponting and Segal 1998). It is unclear who manufactured and wore this type of fibula, but since no fibulas have ever been found in any of the hundreds of Jewish graves excavated in Jerusalem, it is assumed that the person was a local non-Jewish population soldier, involved in the sieges. These fibulas represent a distinctly Near Eastern alloying fashion that was used from the eighth century BCE until Roman times (Ponting 2002a).

When ductile materials are deformed plastically at temperatures much below their melting point, they become stronger. This process is called cold-working (or strain-hardening), and it causes an increase in the dislocation density. When a metal is worked at higher temperatures (hot-working), a little strengthening is achieved since the dislocations can rearrange themselves. However, strain-hardening is not always desirable, since ductility will be reduced. Restoring ductility by removing the effects of strain-hardening can be done by heat treatment, through recovery and recrystallization processes, and may be followed by grain growth. During such a process, strained grains of cold-worked metal are replaced by ordinary equiaxed non-deformed grains, without any dislocation lines. The character of strain-hardening deformation and annealing cycles of Cu-alloy artefacts such as pins, needles, spatulas and fibulas has been well investigated (Sarabia-Herrero *et al*. 1996; Jakielski and Notis 2000; Pinasco *et al*. 2000; Thornton *et al*. 2002; Siano *et al*. 2006; Chiavari *et al*. 2007; Vale'rio *et al*. 2010). A correlation between hardness and recrystallization after heat treatment of cold-worked bronze has been observed by others (Peters 1973). Alloys with high tin content (more than $10 \pm 2.5$ wt% Sn) were kept in their as-cast condition, whereas alloys with low tin contents, used as working tools, were often finished by forging and annealing operations (Vale'rio *et al*. 2010). Lead (Pb) is a common additive to bronze, improving fluidity and castability, but it reduces the alloy's hardness and toughness (Craddock 1977; Giumlia-Mair 1992). Only 2 wt% Pb is needed to produce optimal fluidity, but more than 2 wt% Pb has been found in most Hellenistic and Roman bronze-cast artefacts (Craddock and Giumlia-Mair 1988). The Pb was probably a cheap additive used for economic reasons, although Pb was seldom added in making bronze to be hammered, since it has a deleterious effect on the ductility of the alloy and tends to segregate upon solidification (Craddock and Giumlia-Mair 1988). In such cases, any attempt to perform deformation by hammering will result in the propagation of cracks along the Cu/Pb interface. Another element that may be present in bronze objects is iron (Craddock and Meeks 1987), which exists in copper ore (mainly in copper-iron sulphides). The iron (Fe) could arrive with the flux used during the smelting process (Ingo *et al*. 2006). By the first millennium BCE, Cu smelting in the Middle East had become more efficient and professional (Craddock and Giumlia-Mair 1988). A low iron concentration in the alloy could be a result of efficient copper refining (Vale'rio *et al*. 2010). Iron inclusions are more common in a sophisticated smelting process (Craddock and Giumlia-Mair 1988).

Non-metallic inclusions are usually smaller than 10 μm and normally they are composed of copper with sulphur and some other trace elements (Pinasco *et al*. 2000). It is commonly assumed

that copper containing sulphur was produced by the smelting of chalcopyrite ore (Chernykh *et al*. 1998; Vale'rio *et al*. 2010). The archaeological issue of relating a metallic artefact to a specific ore and origin is very complicated, since the smelting process uses fluxes and fuel (Tylecote *et al*. 1977).

Fibulas were common decorative Cypro-Greek items in Palestine from the Iron Age to the Hellenistic period, with slight, non-chronological typological differences among their various types (Fischer *et al*. 2008). Persian–Hellenistic bow-type fibulas, including spiral ribs on both sides of the bow and a spring catch, were found in the Tel Ya'oz excavation (Fischer *et al*. 2008, with bibliography). Early Near Eastern fibulas (before the eighth century BCE) had an integral bronze pin, but elbow fibulas that were made and used by the Romans were usually manufactured without a pin and spring. In such cases, the pin with the integral spring was made separately and then inserted into the end of the bow socket in the last stage of the manufacturing process. Sometimes iron was used for this purpose, as was observed in one of the Masada elbow fibulas (Ponting 2002a).

There are basic techniques by which metal components were joined together in the Classical Greek and Hellenistic periods. First, the pieces were mechanically fitted together, and then they were metallurgically united by soldering with another metallic alloy having a lower melting point, or they were joined by fusion-welding—pouring molten metal of the same composition into the joint, supplying the energy to melt the two parts locally by diffusion (Craddock 1977). This process was used because two pieces of bronze cannot be connected only by heating and forging, due to the presence of an oxidation layer. In order to bond the two pieces, a bronze wire was heated to the melting point, and then used to connect the two pieces in their local liquid phase (Sarabia-Herrero *et al*. 1996). For Fe/Cu joining, high temperatures must be applied, and may cause an oxidation layer in an oxygen-rich atmosphere. Such a condition may produce an oxidation layer of iron, or 'iron fossil', with a characteristic hardness of 425 HV (Balos *et al*. 2009). Such iron oxide is stable only above 560°C (Fontana 1987; Balos *et al*. 2009), transforming the iron into FeO and $Fe_3O_4$.

The Cu-based artefacts (needle, pins, spatulas and fibulas) examined in this study were retrieved from controlled archaeological excavations at a site in Rishon Le-Zion (Israel) and dated to the first quarter of the third century BCE. The aims of this investigation were to use archaeometallurgical methods in order to determine the composition, microstructure and manufacturing process of these artefacts, and to better understand technological abilities. We also sought to discover whether the objects were produced locally.

## EXPERIMENTAL METHODS

Fourteen artefacts (Fig. 3), found in different locations in the farmhouse (Stratum I), were analysed: one needle, referred to as N1 (Fig. 4 (a)), three pins, referred to as P1–P3 (Figs 4 (b), 4 (c) and 4 (d), respectively), five spatulas, referred to as S1–S5 (Fig. 5), and five fibulas, referred to as F1–F5 (Fig. 6). For this purpose, various methods were used (Table 1): metallographic optical microscopy (OM), scanning electron microscopy with energy-dispersive spectrometry (SEM–EDS), X-ray diffraction (XRD) and microhardness tests.

The needle (N1), 129 mm long, has a circular cross-section, with a sharp tip on one side and an eye on the other side (Fig. 4 (a)). Wear marks were observed on the tip of the needle. All pins have a circular cross-section; the head of pin P1 was preserved, but not its tip (Fig. 4 (b)), whereas the tips of P2 and P3 were preserved, but not their heads (Figs 4 (c) and 4 (d)). The spatulas (S1–S5) have a circular cross-section (Fig. 5); with a flattened side on one edge and a thickened

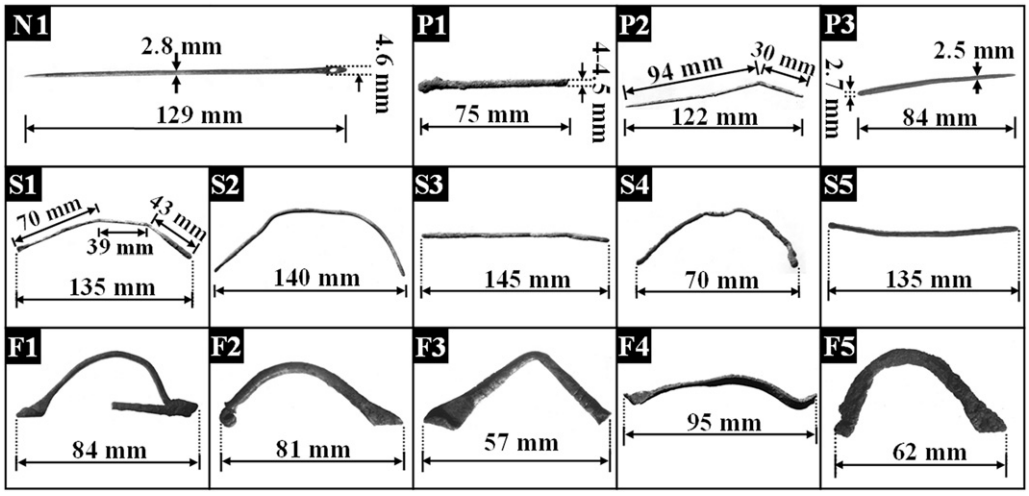


Figure 3 *The 14 bronze artefacts.*

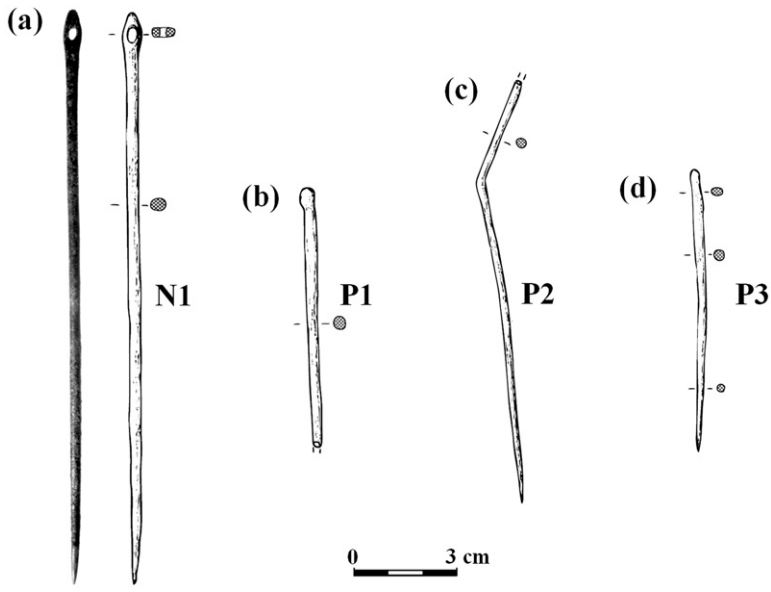


Figure 4 *Photographs of the needle and pins from the Rishon Le-Zion excavations: (a) N1, (b) P1, (c) P2 and (d) P3.*

side on the other edge. Harsh wear and severe corrosion were observed on the flattened side of the spatulas, providing possible clues to the manufacturing process and suggesting that this was the main usable part of the spatulas, although the other (pointed) side of the spatulas may well have functioned for mixing materials. The fibulas (Fig. 6) analysed can be divided into two types: the first has a circular cross-section (CCS) and the second has a rectangular cross-section (RCS), containing a Cu/Fe joint.

All dimensions of the artefacts were measured before the metallographic examination (Fig. 3). A longitudinal cross-section (L-CS), parallel to the surface of the object and perpen-

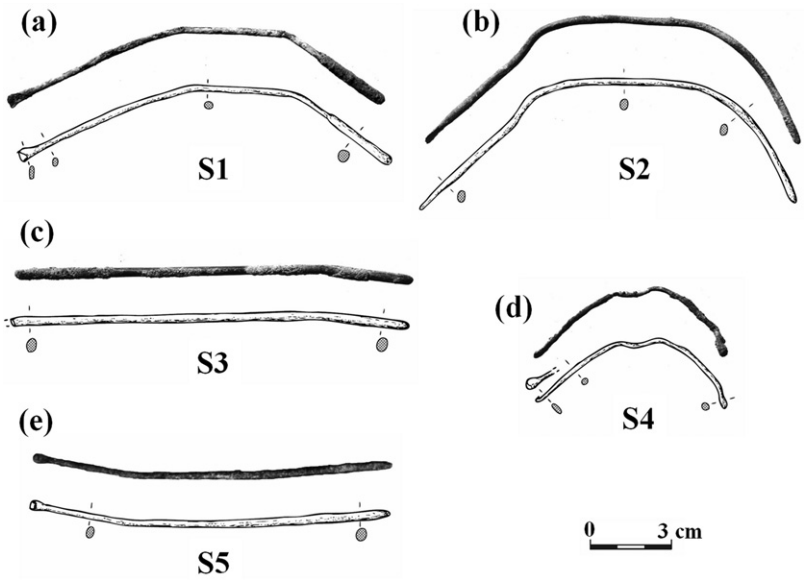


Figure 5 *Photographs of the spatulas from the Rishon Le-Zion excavations: (a) S1, (b) S2, (c) S3, (d) S4 and (e) S5.*

dicular to the cold-worked direction, and a transverse cross-section (T-CS) were cut from different parts of each artefact (according to the ASTM-E3 standard). The samples were mounted in Struers Epofix epoxy resin and were dried at room temperature for 24 h. The preparation of the surface consisted of common metallographic techniques, including grinding with SiC papers (240–600 grits) and then polishing with alumina paste from 5 to 0.05 μm. The samples were then cleaned with ethanol, dried and then etched with iron-chloride acid ($FeCl_3 + HCl + H_2O$). After preparation, the samples were observed under a metallographic OM (ZEISS, AXIO Scope A.1 microscope). Following the metallographic inspection, microhardness tests were performed with a Vickers microhardness test machine (Future-Tech, Microhardness tester, FM-700e), using a diamond indenter with a 50 grf load. SEM imaging was done with an FEI Quanta 200FEG Environmental SEM (ESEM), in high vacuum ($10^{-5}$ mbar) mode, using the Everhart–Thonley secondary electron (SE) detector and an accelerating voltage of 20 kV. The chemical composition was determined by EDS using an Si(Li) liquid-cooled Oxford X-ray detector (detects elements down to boron). X-ray diffraction measurement was performed using a Scintag (USA) powder diffractometer. The scattered radiation was detected by a liquid nitrogen–cooled intrinsic Ge solid-state detector having a high energetic resolution and a low background.

## RESULTS

The OM, ESEM and microhardness test results all indicate that the objects have undergone extensive plastic deformation, resulting in strain-hardening, some annealing cycles and the propagation of cracks. The EDS analysis reveals that all artefacts are made of Cu that contains between 4.9–11.8 wt% Sn (Table 2 (a)).

All specimens had green corrosion on the external surface. Elements such as P, S, Ca, Si, Fe, Al and Cl were observed by EDS analysis at the corrosion layer of the artefacts (Table 2 (b)).

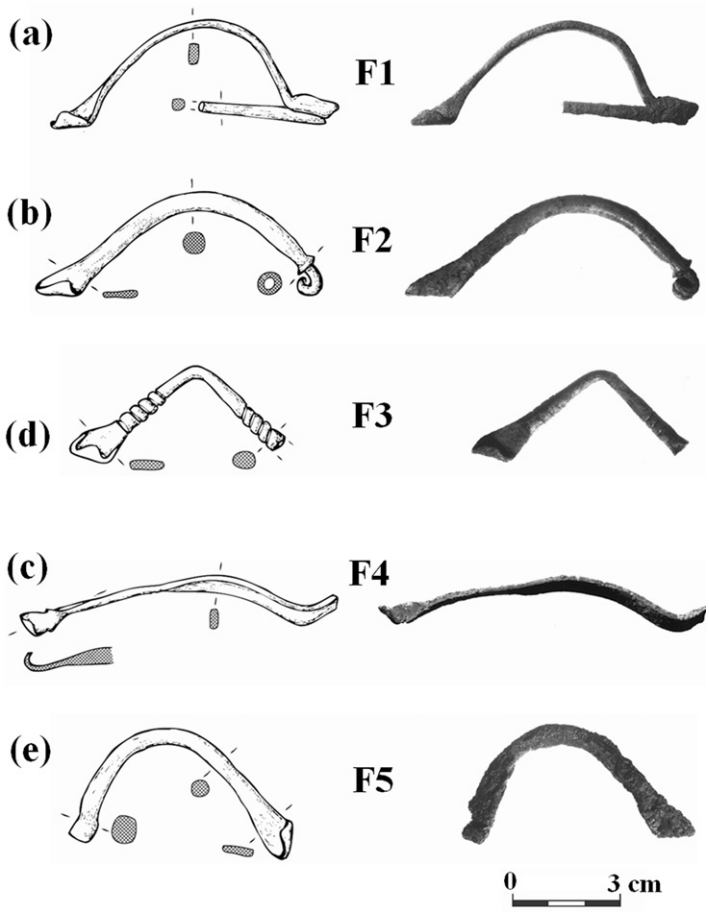


Figure 6 *Photographs of the fibulas from the Rishon Le-Zion excavations: (a) F1, (b) F2, (c) F3, (d) F4 and (e) F5.*

Those are common soil elements (Weinberg *et al*. 1977; Bertholon 2001; Ingo *et al*. 2006; Novakovic *et al*. 2009). There is a strict correlation between soil composition and corrosion products (Robbiola *et al*. 1998; Ingo *et al*. 2006). Repeated cycles of mechanical cold or hot work-hardening with annealing treatments could cause extensive intergranular corrosion phenomena (Ingo *et al*. 2006). The microhardness of specimens P1, S1 and F1 as a function of the distance from the core to the surface is shown in Figure 7.

*Needle*

Metallographic examination of needle N1 reveals cracks and corrosion around the eye (Fig. 8 (a)), an annealing zone including grains (5–35 μm in size) with twins, and a few dislocation slip lines (Fig. 8 (b)), indicating an annealing process. The microhardness test results at the centre of the needle (254.0 ± 28.0 HV) and near the eye's loop (215.0 ± 28.2 HV) are indicative of a high level of strain-hardening due to the cold-working process.

Table 1 *A description of each artefact and the analysis performed on each artefact*

| *Object* | *Type* | *Locus* | *Description* | *OM* | *HV* | *SEM with EDS* | *XRD* |
|---|---|---|---|---|---|---|---|
| N1 | Needle | A/168 | Complete; fairly well preserved; green surface corrosion | + | + | | |
| P1 | Pin | B/083 | Broken tip; fairly well preserved; green surface corrosion | + | + | + | |
| P2 | Pin | A/142 | Broken (the head is missing); fairly well preserved; green surface corrosion | + | + | + | |
| P3 | Pin | B/150 | Broken (the head is missing); bent, fairly well preserved; green surface corrosion | + | + | + | |
| S1 | Spatula | A/093 | Complete; bent; fairly well preserved; green surface corrosion | + | + | + | |
| S2 | Spatula | B/007 | Complete; bent; fairly well preserved; green surface corrosion | + | + | + | |
| S3 | Spatula | A/093 | Complete; fairly well preserved; green surface corrosion | + | + | + | |
| S4 | Spatula | A/022 | Complete; bent; fairly well preserved; green surface corrosion | + | + | + | |
| S5 | Spatula | B/156 | Complete; fairly well preserved; green surface corrosion | + | + | + | |
| F1 | Fibula | A/059 | Almost complete (except for its pin); fairly well preserved; green surface corrosion | + | + | + | + |
| F2 | Fibula | A/168 | Almost complete (except for its pin); fairly well preserved; green surface corrosion | + | + | + | |
| F3 | Fibula | A/168 | Broken; fairly well preserved; green surface corrosion | + | + | | |
| F4 | Fibula | B/084 | Broken; fairly well preserved; green surface corrosion | + | + | + | |
| F5 | Fibula | A/168 | Broken; fairly well preserved; green surface corrosion | + | + | | |

*Pins*

A circumference crack was observed at the head of P1 (Fig. 8 (c)). Grains (20–50 μm) containing dislocation lines were observed on both the head and the tip. The dislocation lines (Fig. 8 (d)) at the pinhead indicate cold-hardening by hammering. At the pin's tip a few twins were observed, which may suggest partial annealing. A longitudinal crack was observed along different parts of P1, perpendicular to the cold-working direction (Fig. 8 (e)). Corrosion and erosion were observed in the pinhead (Fig. 8 (f)). The relatively high microhardness results for P1 ($148.1 \pm 21.9$ HV for the tip and $140.3 \pm 28.2$ HV for the head) indicate cold-working, with partial annealing at the pinhead. It may be seen that the microhardness results for P1 are higher near the external surface than at the core (Fig. 7 (a)). This results from the cold-working process, which leads to less porosity near the external surface of the object.

An edge crack was observed on the T-CS of P2 on both the tip and shaft sides. A longitudinal crack, perpendicular to the cold-working direction, was observed on the L-CS of both the tip and the shaft. Observation of P2 after etching reveals grains (10–50 μm) containing dense dislocation lines. The relatively high microhardness results for P2 ($189.4 \pm 19.7$ HV for the tip and $180.8 \pm 28.8$ HV for the shaft) also indicate a cold-working process on both sides of P2.

A central crack was observed on P3, surrounded by porosity and severe corrosion at the external surface of the sample (Fig. 9 (a); head). Grains 10–40 μm in size, with many dislocation lines, were observed by SEM after etching on both the tip and shaft of P3 (Fig. 9 (b); shaft). The high microhardness values of P3 ($234.2 \pm 24.5$ HV and $205.2 \pm 25.2$ HV for the tip and shaft, respectively) are indicators of strain-hardening due to cold-working.

Table 2 *ESEM–EDS results (values in wt%)*
(a) Using the Quanta 200 ESEM FEG from FEI

| *Artefact* | *Compositions (wt%)* | | | | | |
|---|---|---|---|---|---|---|
| | *Cu* | *Sn* | *O* | *Fe* | *Pb* | *Si* |
| P1 (shaft) | 88.2 | 11.8 | – | – | – | – |
| P2 (shaft) | 90.5 | 9.5 | – | – | – | – |
| P3 (shaft) | 89.4 | 7.5 | 1.7 | – | – | 1.4 |
| S1 (thickened side) | 94.5 | 5.5 | – | – | – | – |
| S1 (flattened side) | 93.4 | 4.9 | 0.9 | – | – | 0.8 |
| S2 (thickened side) | 94.5 | 5.6 | – | – | – | – |
| S2 (flattened side) | 94.1 | 5.9 | – | – | – | – |
| S3 (thickened side) | 95.1 | 4.9 | – | – | – | – |
| S3 (flattened side) | 90.5 | 9.5 | – | – | – | – |
| S4 (thickened side) | 94.6 | 5.4 | – | – | – | – |
| S5 (flattened side) | 94.4 | 5.6 | – | – | – | – |
| Fl (Cu, bulk) | 91.0 | 9.0 | – | – | – | – |
| Fl (Cu, bulk) | 92.8 | 7.2 | – | – | – | – |
| Fl (Fe oxide) | – | – | 38.8 | 61.2 | – | – |
| F2 (Cu, bulk) | 90.4 | 9.6 | – | – | – | – |
| F2 (Cu, bulk) | 90.6 | 9.4 | – | – | – | – |
| F2 (Cu, bulk) | 89.1 | 8.3 | – | – | 2.6 | – |
| F4 (Cu, bulk) | 92.6 | 7.4 | – | – | – | – |
| F4 (Fe oxide) | 6.3 | – | 15.9 | 77.8 | – | – |

(b) At the corrosion layer

| *Artefact* | *Compositions (wt%)* | | | | | | | | | | |
|---|---|---|---|---|---|---|---|---|---|---|---|
| | *Cu* | *Sn* | *O* | *Cl* | *S* | *Fe* | *Al* | *Si* | *Ca* | *Mg* | *Pb* |
| S4 | 80.8 | 7.8 | 5.5 | 0.9 | – | 0.8 | – | – | – | – | 4.3 |
| S4 | 70.6 | 12.5 | 6.5 | 1.9 | – | 1.0 | 2.6 | – | – | – | 4.8 |
| S4 | 87.6 | 4.5 | 4.3 | 1.8 | – | – | 1.8 | – | – | – | – |
| Fl | 39.9 | 3.8 | 14.3 | – | 1.1 | 39.7 | – | 1.3 | – | – | – |
| Fl | – | – | 37.7 | – | – | 2.3 | 0.7 | 6.9 | 35.6 | 0.9 | – |
| Fl | 63.6 | 4.1 | 4.1 | 7.2 | 3.1 | 17.9 | – | – | – | – | – |
| F2 | 48.6 | – | 30.0 | – | – | – | 7.0 | 14.4 | – | – | – |
| F2 | 47.6 | – | 25.0 | 0.8 | – | – | 3.4 | 23.2 | – | – | – |
| F2 | 58.2 | 26.3 | 9.6 | 4.1 | – | – | 1.9 | – | – | – | – |
| F4 | 80.9 | 6.7 | 5.6 | – | – | – | – | – | – | – | 6.9 |
| F4 | 3.6 | – | 18.1 | – | – | 64.2 | – | 0.7 | 13.5 | – | – |
| F4 | 3.7 | – | 18.5 | – | – | 70.4 | – | – | 7.4 | – | – |
| F4 | 90.2 | 1.8 | 6.8 | – | – | – | – | 1.2 | – | – | – |

## *Spatulas*

A thick corrosion layer was observed on the external surface of the flattened side of S1, with a circumference crack at the corrosion layer. This circumference crack is similar to the crack

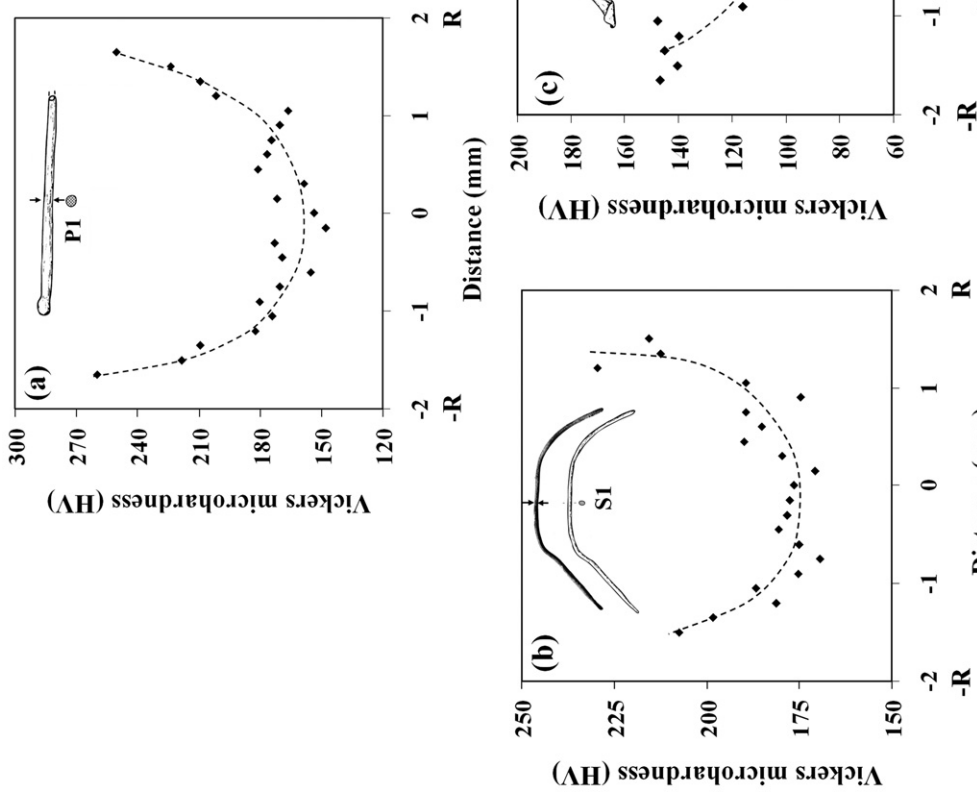


Figure 7 *Microhardness results for selected artefacts (T-CS) as a function of the distance from the core to the surface: (a) specimen P1, (b) specimen S1 and (c) specimen F1.*

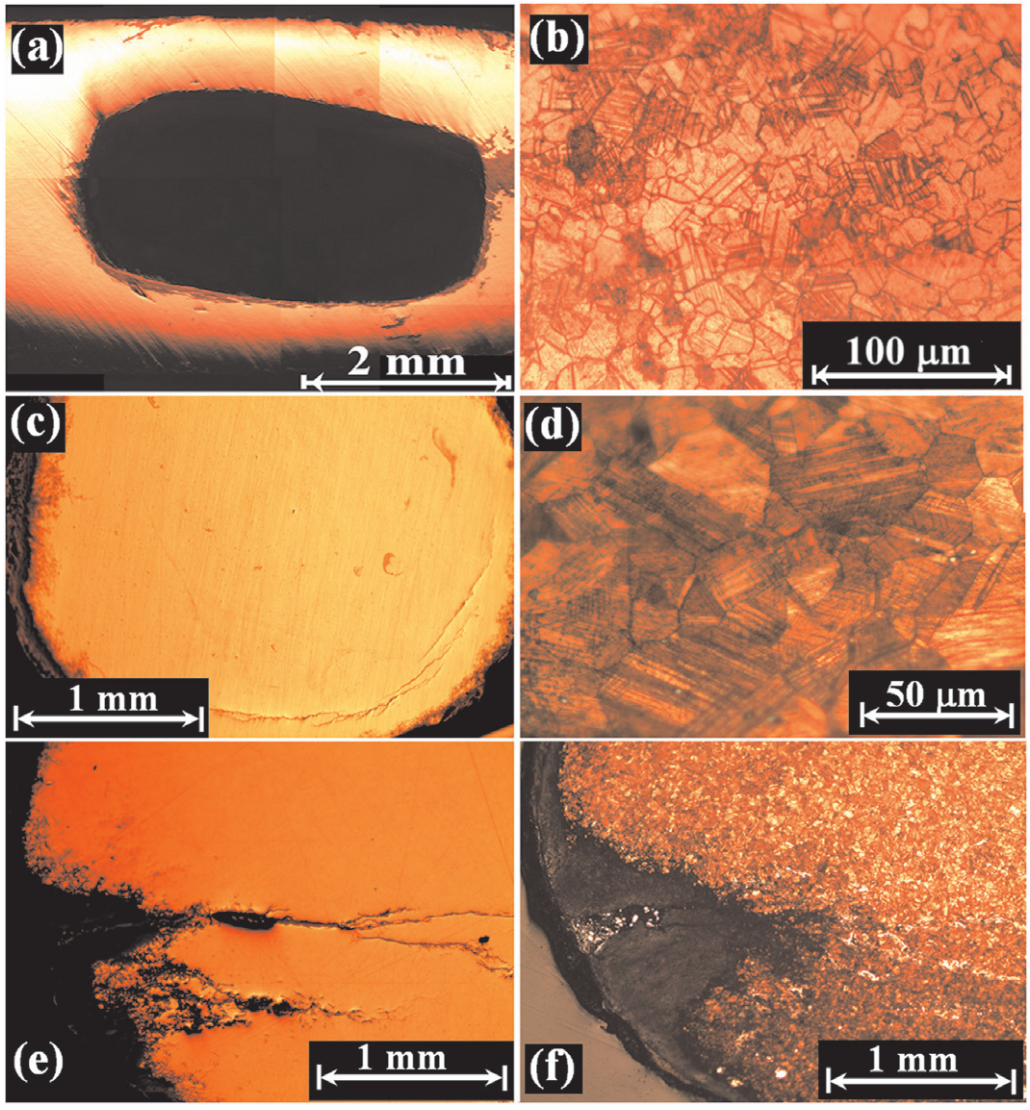


Figure 8 *Metallographic examination (OM) of N1 and P1 reveals: (a) corrosion at the L-CS of the needle eye; (b) a few dislocation lines and twins at the L-CS of the N1 eye after etching; (c) a circumference crack at the T-CS of the P1 head; (d) dislocation lines at the L-CS of the P1 head after etching; (e) cracks at the L-CS of the P1 head; and (f) wear at the L-CS of the P1 head after etching.*

observed on P1 (Fig. 8 (c)). Grains 5–25 µm in size, with many dislocation lines, were observed by SEM on the flattened and thickened sides of S1 (Fig. 10 (a); flattened side). The microhardness of S1 (183.3 ± 10.8 HV and 152.2 ± 32.3 HV for the flattened and thickened sides, respectively) is an indictor of a strain-hardening process. It may be seen that the microhardness of S1 is higher near the external surface and lower at the core (Fig. 7 (b)). This condition is typical of the process of cold-working, which leads to dense dislocation lines and less porosity near the external surface.

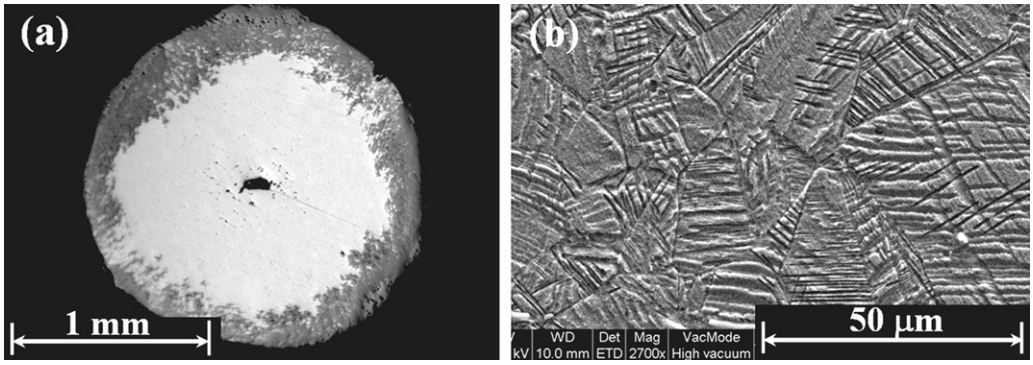


Figure 9 *Metallographic examination of pin P3 reveals: (a) a central crack, porosity and a corrosion layer at the T-CS of the tip of P3 (OM); and (b) dislocation lines at the L-CS of the shaft of the pin of P3 after etching (SEM).*

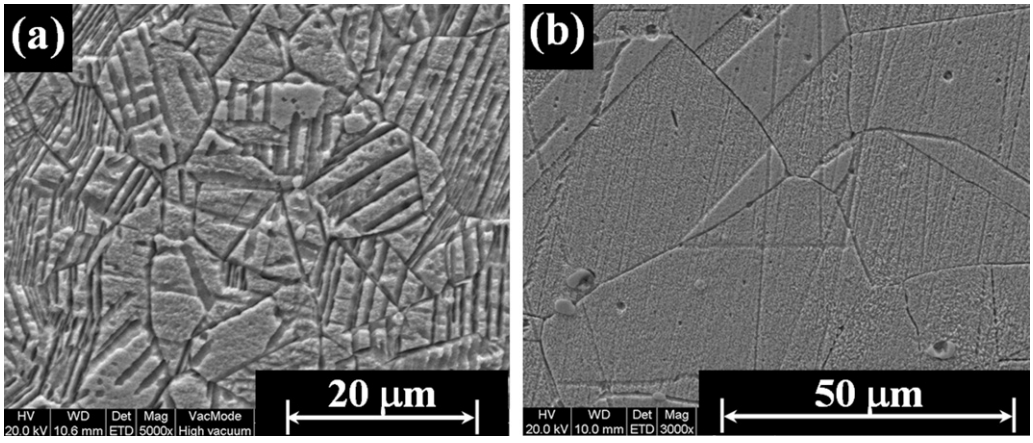


Figure 10 *Metallographic examination (SEM) of S1 and S2 reveals: (a) grains with many dislocation lines, as at the S1 flattened side after etching the L-CS; and (b) an annealing zone with twins (L-CS) at the thickened side of S2 after etching, including inclusions composed of sulphur and iron.*

An edge crack was observed at the T-CS along the thickened side of S2. A similarly shaped crack was also observed on P2. An annealing zone, with large grains (30–70 μm) and twins, was observed by SEM at the thickened side of S2, and included inclusions (Fig. 10 (b)). The inclusions identified by EDS contained 74.5 wt% Cu, 1.8 wt% Sn, 18.9 wt% S and 4.8 wt% Fe. Sulphur and iron inclusions have also been observed in other archaeological studies of bronze artefacts (Chernykh *et al*. 1998; Pinasco *et al*. 2000; Ingo *et al*. 2006; Vale'rio *et al*. 2010), and may indicate the manufacturing process of the copper alloy as well as its provenance. The low values of the microhardness test results for S2 ($107.9 \pm 8.0$ HV and $96.5 \pm 9.0$ HV for the flattened and thickened edges, respectively) are indicators of an annealing process.

Grains 5–20 μm in size, with many dislocation lines, were observed on S3 after etching on both the T and L cross-sections of the flattened and thickened edges.

On the thickened side of S4, severe corrosion, high porosity and a central crack were observed (Fig. 11 (a)), with a longitudinal crack similar to that of P2. Annealing twins and

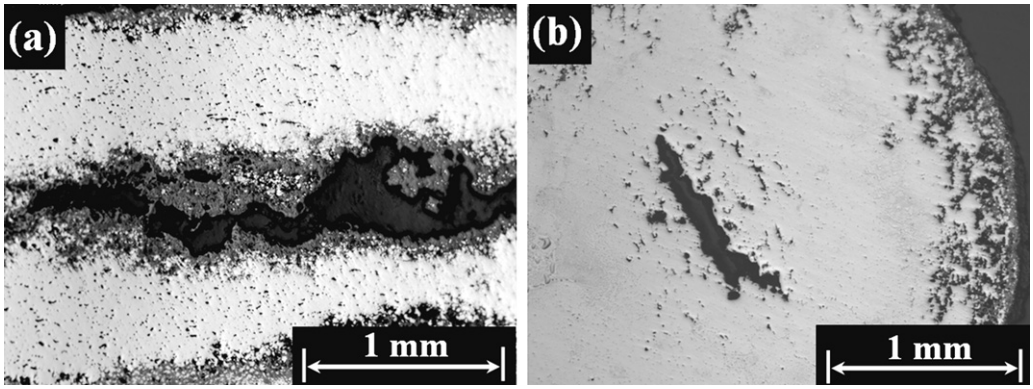


Figure 11 *Metallographic examination (OM) of the S4 and S5 spatulas before etching reveals: (a) a central/longitudinal crack, high porosity and a thick corrosion layer (L-CS) of the thickened side of S4; and (b) a central crack surrounded by porosity and a thick corrosion layer on the external surface (T-CS) of the thickened side of S5.*

large grains (50 μm size) were observed on the thickened side after etching. A thick corrosion layer, high porosity and a circumference crack were observed on the external surface of S4, with a crack similar to that of P1 and S1 (Fig. 8 (c)). Grains 25–50 μm in size and twins were observed on S4 after etching of the flattened side. The EDS analysis of the external surface of S4 reveals the presence of Cu and Sn, with additions of elements such as O, Cl, Fe and Al (Table 2 (b)), which are typical corrosion products and soil elements. The presence of Pb was observed on the corroded surface of S4. A central crack (similar to the crack observed on pin P3—Fig. 9 (a)) was observed on the flattened side of S5. High porosity resulting from the casting and the corrosion processes was also observed on the external surface of S5's flattened edge (Fig. 11 (b)).

The microhardness results for S3 ($139.4 \pm 7.3$ HV and $130.9 \pm 8.8$ HV for the flattened and thickened sides, respectively), are indicators of strain-hardening, whereas the microhardness results for S4 ($105.8 \pm 11.0$ HV and $94.4 \pm 9.1$ HV for the flattened and thickened edges, respectively), and S5 ($120.6 \pm 22.6$ HV and $104.5 \pm 9.2$ HV for the flattened and thickened sides, respectively) are indicators of a recrystallization process combined with high porosity.

### *Fibulas*

Both F1 and F4 have a rectangular cross-section (RCS) with a Cu/Fe joint, while F2, F3 and F5, which are similar typologically to the Masada Roman elbow fibulas examined by others (Ponting 2002a), have a circular cross-section (CCS), with a Cu/Cu joint. The RCS fibulas have a ferrous pin connected to the bow in a pre-prepared hole at its edge. Such a bimetallic device is sensitive to galvanic corrosion, as observed in both F1 (Fig. 12 (b)) and F4 (see Fig. 14 below). The CCS fibulas have a bronze pin with a twisted head, which is fixed to the bow on one side by placing it in a pre-prepared cavity in the bow and pressing the bow around the cavity with pliers (Ponting 2002a). The pins of the Rishon Le-Zion fibulas themselves did not survive and were probably broken at the twisted part. The area around the twisted part was subject to significant stresses during the manufacturing process of the fibulas and in their daily use.

The EDS analysis of the F4 iron oxide (Table 2 (a)) reveals the presence of Fe and O. The XRD results for the iron oxide in specimen F1 reveal the presence of goethite, maghemite,

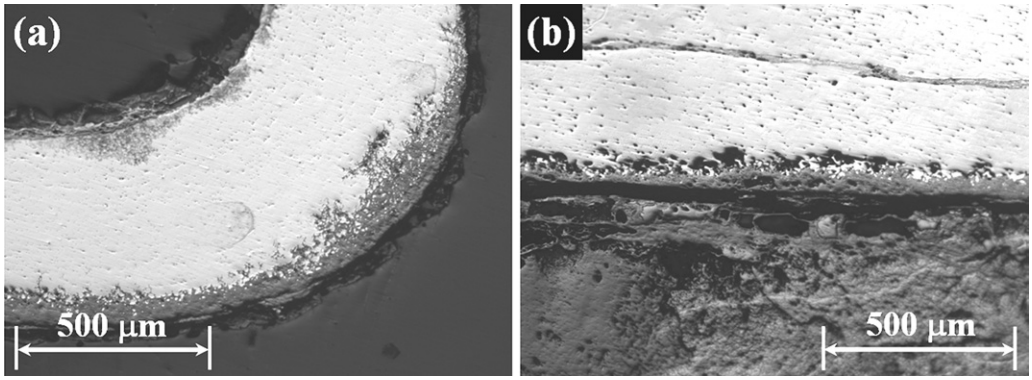


Figure 12 *Metallographic examination of the F1 RCS fibula reveals: (a) severe corrosion at the bending zone (OM), resulting from plastic deformation; and (b) the interface between the bronze fibula bow and the iron spring (OM), and a crack in the bronze, parallel to the joining interface.*

lepidocrocite, wustite and iron–cobalt–silicon. Lepidocrocite and goethite may be corrosion products as well as products found in the consolidation of an iron bloom, whereas wustite (FeO) is not expected during low-temperature corrosion, since it is not stable at temperatures below 570°C. This may indicate a sophisticated joining technique for copper and iron.

On the bronze part of F1, corrosion was observed on the bending zone (Fig. 12 (a)), resulting from plastic deformation and residual stresses. High porosity was observed on F1, resulting from the casting process. The EDS analysis of the F1 joint reveals the presence of Cu, Sn and Fe, with additions of elements such as O, Cl, Al, S, Si, Ca and Mg (Table 2 (b)), which are typical corrosion products and soil elements. A bonding zone was revealed by OM (Fig. 12 (b)). Between the bronze fibula and the iron spring, a crack was also observed (Fig. 12 (b)), parallel to the joining interface. A recrystallized zone with a grain size of 40–60 μm, dislocation lines and twinned grains were observed. The low microhardness values (98.7 ± 11.4 HV) of the Cu bulk of F1 indicate a recrystallization process. It may be seen that the microhardness results along the T-CS of F1 are higher near the external surface and lower at the core (Fig. 7 (c)). This condition results from the cold-working process. The high microhardness values (541.1 ± 61.4 HV) of the Fe bulk match the hardness of FeO and $Fe_3O_4$ (Balos *et al*. 2009).

Severe corrosion was observed on the bending area of F2, resulting from the plastic deformation during cold-working. The EDS analysis of the F2 joint reveals the presence of Cu and Sn, with additions of elements such as O, Cl, Al and Si (Table 2 (b)), which are typical corrosion products and soil elements. Cracks were observed on the bending area of the loop connecting the bronze spring and the bronze arc (Fig. 13 (a)). Dislocation slip lines and twins were observed near the bending zone, using OM (Fig. 13 (b)), as well as inclusions identified by the EDS as 76.5 wt% Cu, 20.8 wt% S and 2.7 wt% Fe. An annealing zone, with large grains (30–70 μm) and twins, was observed at the L-CS of F2 after etching. The microhardness results for F2 reveal the greater hardness of the copper alloy near the interface connecting the bronze spring and the bronze arc (153.5 ± 48.9 HV) than in the bulk of the arc (104.5 ± 10.3 HV), which may have resulted from the intensive work-hardening process at the bonding zone between the spring and the arc. An annealing zone was observed on F3 near the Cu/Cu interface, including grains (20–40 μm) with twins, indicating an annealing process.

The metallographic observation of fibula F4 revealed a joining zone (Fig. 14) between the bronze fibula and the iron spring. The bronze grains near the iron/bronze interface contain

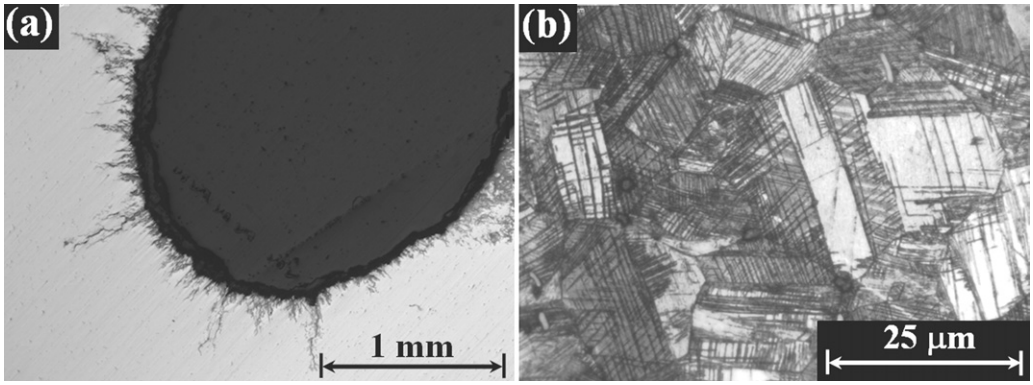


Figure 13 *Metallographic examination (OM) of the F2 CCS fibula reveals: (a) cracks at the bending area of the loop connecting between the bronze spring and the bronze arc; and (b) dislocation lines and twins near the bending zone (after etching).*

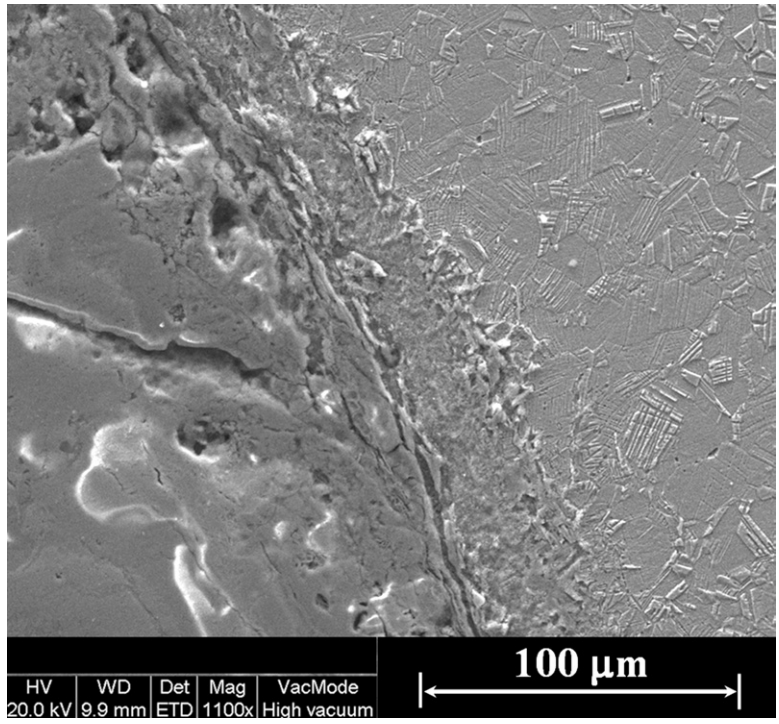


Figure 14 *Metallographic examination of the F4 RCS fibula reveals the iron/bronze joining zone (SEM, after etching).*

dislocation slip lines, with a grain size of 10–30 μm. The EDS analysis of F4 iron oxide reveals the presence of Fe, O and Cu (Table 2 (a)). The EDS analysis of the F4 joint reveals the presence of Cu, Sn, Fe and additions of elements such as O, Si and Ca (Table 2 (b)), which are typical corrosion products and soil elements. The microhardness results for F4 reveal the greater

hardness of the bronze near the interface connecting the bronze and iron (152.8 ± 12.0 HV) than in the bulk of the bronze arc (100.7 ± 2.9 HV), which may have resulted from the work-hardening of the fibula near the bonding zone.

Metallographic examination of fibula F5 at the L-CS after etching reveals an annealing zone including grains (20–50 μm) with twins and few dislocation slip lines. The microhardness test results for F5 reveal a hardness of 126.0 ± 23.2 HV at the area connecting the bronze spring and the bronze arc, and 129.7 ± 23.0 HV at the copper arc, which indicates some work-hardening.

## SUMMARY AND CONCLUSIONS

The importance of the present study lies in the absence of studies on Eastern Mediterranean Hellenistic bronzes. The results show that the assemblage of metal objects found at Rishon Le-Zion was made of good-quality melted binary tin bronzes, composed of copper with a tin composition of between 2.4–11.8 wt% Sn and slight amounts of impurities. These copper alloys were probably selected according to the artefact's functionality (mechanical properties), since functional working tools require ductility as well as great strength. Higher Sn concentrations (above ~14 wt%) would make the alloy more brittle and difficult to work with (Vale'rio *et al*. 2010). The ancient metalworker was probably taking into account sets of other criteria, such as fashion and status (Ponting 2002a,b).

Casting defects such as pores have been observed on some of the artefacts. Thermomechanical processes of hammering and annealing were applied in the manufacturing of the artefacts; all the objects underwent extensive plastic deformation, resulting in strain-hardening (dislocation lines, propagation of some cracks and a high degree of hardness). A few of the artefacts (the area around the eye of needle N1, three of the spatulas and some areas of the fibulas) underwent annealing cycles as well, resulting in annealing twins. Annealing restores ductility lost during hammering, and thereby enables further deformation of the object (Vale'rio *et al*. 2010). The pins, spatulas and needle were manufactured according to the same production technique, using a similar Cu–Sn bronze alloy and shaping the objects by the process of cold-working. Metallurgical knowledge and skills in the forging and annealing processes could compensate for casting problems (Sarabia-Herrero *et al*. 1996). Although the fibulas were manufactured by a somewhat similar method, their production was more complicated, since joining techniques were used to bond the body and pin of the fibulas.

These results may also assist us in defining the original function of the metal objects. The dimensions of the needle (129 mm), as well as its relatively high degree of hardness (254.0 ± 28.0 HV at the centre of the needle), may suggest that it was used for leather work. The dimensions of the pins (P2 and P3 originally measured more than 124 mm), as well as the wear marks on their tips, and the relatively high degree of hardness (e.g., 189.4 ± 19.7 HV at the tip of P2), may suggest that they were also used for leather work (the possibility that the pins were surgical instruments, a function often suggested for these objects in the archaeological literature, cannot be ruled out altogether). All spatulas examined have a long stem (e.g., S1 originally measured more than 150 mm in length) and they were probably used for mixing and spreading various materials, among which were pharmaco-cosmetic products, pigment powders, adhesives and the like. The annealing processes seen in some of the spatulas (S2, S4 and S5) may have been related to their use. The fibulas are the most interesting objects analysed in the assemblage. Two types of fibulas were differentiated according to morphology and material, the first (RCS) with a Cu/Fe joint (F1 and F4), and the second (CCS) with a Cu/Cu joint (F2, F3 and F5). One cannot reject the idea that different materials served different (practical) functions; for example, to fasten

clothes, as opposed to the use of a safety pin. Moreover, the fact that all the fibulas with the Cu/Cu joints (F2, F3, F5) came from the same room (Locus 168; Fig. 2) lends support to such a conclusion. The analysed microhardness of the iron oxide zone of fibula F1 matches the composition of FeO and $Fe_3O_4$ (Balos *et al*. 2009). Such iron oxides are the consequence of a high-temperature fire environment (Fontana 1987; Balos *et al*. 2009).

The fact that all artefacts are securely dated to within half a century, the 320s to 270s BCE (at most), suggests that these different manufacturing technologies coexisted. The idea that all were made from a similar ore may also suggest a workshop that practised these techniques together, possibly locally. Additional investigation is recommended in the future, including quantified minor and trace elements, as well as non-destructive radiographic tests and a future study of the joining part between the iron pin and the bronze fibula bow.

The metallographic, chemical and microhardness examinations of the Hellenistic bronze objects retrieved from Rishon Le-Zion allow the identification of the microstructure and composition of the alloys. The artefacts were manufactured from a binary copper bronze alloy with appropriately 4.9–11.8 wt% Sn, which means that the alloy composition was carefully controlled

Table 3 *The manufacturing processes of the artefacts*

| *Artefact* | *Type* | *Manufacturing process* |
|---|---|---|
| N1 | Needle | Cast and cold-worked; the high hardness values indicate a cold-hardening process; the twins and a few dislocation lines at the eye of the needle indicate cold-hardening and annealing processes |
| P1 | Pin | Cast and cold-worked; the circumference crack, dislocation slip lines and high hardness values indicate a cold-hardening process, with partial annealing at the pin head |
| P2 | Pin | Cast and cold-worked; the central crack, a high density of dislocation lines and high hardness values indicate a cold-hardening process |
| P3 | Pin | Cast and cold-worked; many dislocation lines and high hardness values indicate a cold-hardening process |
| S1 | Spatula | Cast and cold-worked; the circumference crack and high hardness values indicate a cold-hardening process |
| S2 | Spatula | Cast, cold-worked and annealed; the cracked edge, recrystallized zone with large grains, twins and low hardness values indicate cold-hardening and annealing processes |
| S3 | Spatula | Cast and cold-worked; the circumference crack and high hardness values indicate a cold-hardening process |
| S4 | Spatula | Cast, cold-worked and annealed; a central crack and low hardness values indicate cold-hardening and annealing processes |
| S5 | Spatula | Cast, cold-worked and annealed; a central crack and low hardness values indicate cold-hardening and annealing processes |
| F1 | Fibula (RCS) | Cast, Fe/welded interface, cold-worked and annealed; the recrystallized zone with large grains, twins and low hardness values indicate cold-hardening and annealing processes |
| F2 | Fibula (CCS) | Cast, Cu/Cu joint and cold-worked with bronze pin with a twisted head; the many dislocation lines and high hardness values indicate a cold-hardening process |
| F3 | Fibula (CCS) | Cast, Cu/Cu joint and cold-worked bronze pin with a twisted head; the high hardness values indicate a cold-hardening process |
| F4 | Fibula (RCS) | Cast, Fe/Cu welded interface, cold-worked and annealed; the bronze grains near the iron/bronze interface contain dislocation slip lines and high hardness, and the bronze grains far from the iron/bronze interface contain twins and low hardness values, indicating cold-hardening and annealing processes |
| F5 | Fibula (CCS) | Cast, Cu/Cu joint and cold-worked bronze pin with a twisted head |

and the metals were not recycled. Thermomechanical operations were applied during the manufacturing process of the objects, according to the artefact's functionality. Task-oriented tools such as needles, pins and spatulas were produced by work-hardening and annealing cycles, using smiths' tools. These results provide a better understanding of the characterization of Early Hellenistic metal objects in Palestine and reveal the metallurgical manufacturing process of those artefacts. The fact that all of the analysed artefacts were manufactured from a similar bronze alloy and shaped by cold-working (Table 3) may indicate that they were all manufactured at the same workshop; given the availability of the bronze, it might have been local. Furthermore, we conclude that the manufacturing process of the fibulas included sophisticated Fe/Cu joining techniques (Figs 12 and 14), since the XRD results for iron oxide in fibula F1 reveal the presence of wustite (FeO), which is not stable below 570°C. All these technological characteristics point towards advanced metallurgical knowledge and expertise. The presence of fibulas at the site enhances our knowledge of their use among the non-Jewish populations of Classical periods in Palestine (cf., Ponting 2002a, 561, for the Early Roman period). We have clear historical and epigraphic evidence that the site's geographical and ethnic setting during the Persian and Early Hellenistic periods was predominantly Phoenician, probably under Sidonian hegemony (cf., e.g., Gitler and Tal 2006, 43–6). Combining the archaeological evidence and the results of the metallurgical testing, it may be concluded that the copper ore originated from an Eastern Mediterranean (probably Near Eastern) region. This may give us additional information regarding the Hellenistic economy and trade trends. Only further examination of slag, crucibles and ore materials, which have not yet been found at this Rishon Le-Zion site, may yield more definitive conclusions.

## ACKNOWLEDGEMENTS

The authors wish to thank Mario Levinstein from the School of Mechanical Engineering at Tel Aviv University and Zahava Barkai and Yuri Rosenberg from the Wolfson Applied Materials Research Center, at Tel Aviv University, for their assistance. The authors also wish to thank the anonymous reviewers, who offered important comments on the previous versions of this paper.

## REFERENCES

Balos, S., Benscoter, A., and Pense, A., 2009, Roman mystery iron blades from Serbia, *Materials Characterization*, **60**, 271–6.

Bertholon, R., 2001, The original surface of corroded metallic archaeological objects: characterization and location, *La Revue de Métallurgie*, No. 9 (September), 817–23.

Chernykh, E. N., Prusakov, B. A., and Katkova, L. V., 1998, A study of ancient copper, *Metals Science and Heat Treatment*, **40**(9–10), 368–73.

Chiavari, C., Degli Esposti, M., Garagnani, G. L., Martini, C., Prandstraller, D., and Trocchi, T., 2007, Bronze archaeological finds from the Villanovan Necropolis of Orto Granara (BO): study of manufacturing technologies and evaluation of the conservation state, *La Metallurgia Italiana*, Maggio, 43–52.

Craddock, P. T., 1977, The composition of the copper alloys used by the Greek, Etruscan and Roman civilisations: 2. the archaic, classical and Hellenistic Greeks, *Journal of Archaeological Science*, **4**, 103–23.

Craddock, P. T., and Giumlia-Mair, A., 1988, Problems and possibilities for provenancing bronzes by chemical composition, in *Bronzeworking centres of Western Asia, c. 1000–539 B.C.* (ed. J. Curtis), 317–26, Kegan Paul International in association with the British Museum, London.

Craddock, P. T., and Meeks, N. D., 1987, Iron in ancient copper, *Archaeometry*, **29**, 187–204.

Fischer, M., Roll, I., and Tal, O., 2008, Persian and Hellenistic remains at Tel Ya'oz, *Tel Aviv*, **35**, 123–63.

Fontana, M. G., 1987, *Corrosion engineering*, 3rd edn, 508–9, McGraw-Hill, New York.

Friedman, E. S., Brody, A. J., Young, M. L., Almer, J. D., Segre, C. U., and Mini, S. M., 2008, Synchrotron radiation-based X-ray analysis of bronze artifacts from an Iron Age site in the Judean Hills, *Journal of Archaeological Science*, **35**, 1951–60.

Gitler, H., and Tal, O., 2006, *The coinage of Philistia of the fifth and fourth centuries BC: a study of the earliest coins of Palestine*, Collezioni Numismatiche 6, Ennerre, Milan.

Giumlia-Mair, A., 1992, The composition of copper-based small finds from a west Phoenician settlement site and from Nimrud compared with that of contemporary Mediterranean small finds, *Archaeometry*, **34**, 107–19.

Giumlia-Mair, A., 2005, Copper and copper alloys in the southeastern Alps: an overview, *Archaeometry*, **47**, 275–92.

Ingo, G. M., De Caro, T., Riccucci, C., Angelini, E., Grassini, S., Balbi, S., Bernardini, P., Salvi, D., Bousselmi, L., Cilingiroglu, A., Gener, M., Gouda, V. K., Al Jarrah, O., Khosroff, S., Mahdjoub, Z., Al Saad, Z., El-Saddik, W., and Vassiliou, P., 2006, Large scale investigation of chemical composition, structure and corrosion mechanism of bronze archaeological artefacts from Mediterranean basin, *Applied Physics A*, **83**, 513–20.

Jakielski, K. E., and Notis, M. R., 2000, The metallurgy of Roman medical instruments, *Materials Characterization*, **45**, 379–89.

Meeks, N. D., 1986, Tin-rich surfaces on bronze—some experimental and archaeological considerations, *Archaeometry*, **28**, 133–62.

Novakovic, J., Papadopoulou, O, Vassiliou, P., Filippaki, E and Bassiakos, Y., 2009, Plasma reduction of bronze corrosion developed under long-term artificial ageing, *Analytical and Bioanalytical Chemistry*, **395**, 2235–44.

Oron, A., 2006, The Athlit ram bronze casting reconsidered: scientific and technical re-examination, *Journal of Archaeological Science*, **33**, 63–76.

Peters, B. F., 1973, The evolution of annealing textures in a heavily-deformed bronze, *Metallurgical Transactions*, **4**, 757–63.

Pinasco, M. R., Stagno, E., Ienco, M. G., Piccardo, P., Macellari, R., and Fiori, F., 2000, Manufacturing fifth century B.C. Certosa brooches, *Journal of the Minerals, Metals and Materials Society*, **52**(6), 13–15.

Ponting, M. J., 2002a, Roman military copper-alloy artefacts from Israel: questions of organization and ethnicity, *Archaeometry*, **44**, 555–71.

Ponting, M. J., 2002b, Keeping up with the Romans? Romanization and copper alloys in First Revolt Palestine, *IAMS Newsletter*, **22**, 3–6.

Ponting, M. J., and Segal, I., 1998, ICP–AES analyses of Roman military copper-alloy artefacts from the excavations at Masada, Israel, *Archaeometry*, **40**, 109–22.

Robbiola, L., Blengino, J. M., and Fiaud, C., 1998, Morphology and mechanisms of formation of natural patinas on archaeological Cu–Sn alloys, *Corrosion Science*, **40**(12), 2083–111.

Rovira, S., and Montero, I., 2003, Natural tin–bronze alloy in Iberian Peninsula metallurgy: potentiality and reality, in *The problem of early tin* (eds. A. Giumlia-Mair and F. Lo Schiavo), 15–22, Archaeopress, Oxford.

Sarabia-Herrero, E. J., Martin-Gil, J., and Martin-Gil, F. J., 1996, Metallography of ancient bronzes: study of pre-Roman metal technology in the Iberian peninsula, *Materials Characterization*, **36**, 335–47.

Siano, S., Bartoli, L., Santisteban, J. R., Kockelmann, W., Daymond, M. R., Miccio, M., and Marinis, G. D., 2006, Non-destructive investigation of bronze artefacts from the Marches National Museum of Archaeology using neutron diffraction, *Archaeometry*, **48**, 77–96.

Srinivasan, S., 1998, The use of tin and bronze in prehistoric southern Indian metallurgy, *Journal of Metals*, **50**(7), 44–9.

Tal, O., 2005, Persian remains at Rishon Le-Zion, *Salvage Excavation Reports*, **2**, 30–7.

Tal, O., 2009, On the identification of the ships of *kzd/ry* of the erased Customs Account from Elephantine, *Journal of Near Eastern Studies*, **68**, 1–8.

Thornton, C. P., Lamberg-Karlovsky, C. C., Liezers, M., and Young, S. M. M., 2002, On pins and needles: tracing the evolution of copper-base alloying at Tepe Yahya, Iran, via ICP–MS analysis of common-place items, *Journal of Archaeological Science*, **29**, 1451–60.

Tylecote, R. F., Ghaznavi, H. A., and Boydell, P. J., 1977, Partitioning of trace elements between the ores, fluxes, slags and metal during the smelting of copper, *Journal of Archaeological Science*, **4**, 305–33.

Vale'rio, P., Silva, R. J. C., Soares, A. M. M., Arau'jo, M. F., Fernandes, F. M. B., Silva, A. C., and Berrocal-Rangel, L., 2010, Technological continuity in early Iron Age bronze metallurgy at the south-western Iberian Peninsula—a sight from Castro dos Ratinhos, *Journal of Archaeological Science*, **37**, 1811–19.

Weinberg, F., Jacobson, D. M., and Pelleg, J., 1977, An investigation of ancient metal objects from the north Sinai Coast, *Metallography*, **10**, 171–8.